physica status solidi a
www.pss-a.com

Sputter Deposition of Transition Metal Oxides on Silicon: Evidencing the Role of Oxygen Bombardment for Fermi-Level Pinning

*Raphaël Poulain, Joris Proost, and Andreas Klein**

Different magnetron sputtering-based deposition methods of nickel oxide SiO_2-passivated Si surfaces are compared. Results highlight that the presence of oxygen in the deposition chamber during reactive sputtering drastically affects the Si/SiO_2 interface. An alternative method for the preparation of NiO is the sputtering of metallic nickel in oxygen-free atmosphere followed by a post oxidation of the deposited layer in an oxygen atmosphere without plasma exposition is proposed. This method is introduced as metal layer oxidation (MLO). Using this technique, the barrier height on n-type silicon increases from ≈0.4 eV for reactively sputtered NiO to more than 0.6 eV for the MLO method. In situ photoelectron spectroscopy evidences the formation of an extra electronic state when NiO is reactively sputtered, which is assigned to the intense oxygen ion bombardment of the Si/SiO_2 surface during the process. This extra-electronic state pins the silicon energy bands in an undesirable position. The extra-electronic state is associated with oxygen interstitial in the SiO_2 implanted during reactive sputtering.

1. Introduction

Transition metal oxides (TMOs) provide a wide set of material properties with varying work functions and band gaps. Recently, the interest in interfacing TMOs with silicon has substantially increased. Silicon/TMO structures can be encountered not only in water-splitting devices where the TMO layer is a catalytic layer,[1,2] but also in solid-state junction where the TMO layer could be implemented for creating a charge-selective contact[2–9]. For instance, n-type materials as TiO_2 and ZnO could be implemented to create electron-selective contacts on silicon,[5,6] whereas p-type materials or high-work-function materials, such as MoO_3, WO_3, V_2O_5, and NiO, could be implemented to create hole-selective contacts.[2,7,8] The literature on TMO deposition would suggest that soft deposition methods, such as atomic layer deposition (ALD), thermal evaporation, pulse laser deposition, or solution-based deposition, would be the most adequate for depositing a TMO layer on a photoactive material.[6,10–12] In contrast, sputtering or e-beam evaporation deposition might damage the silicon surface and reduce the interface quality.[2,3,13–15]

Regarding the sputtering technique, Ellmer and Welzel have shown that negative-ion bombardment (e.g., by oxygen ions) in the chamber of deposition can have significant consequences.[16] In contrast to other particles having kinetic energy in the 1–20 eV range, the negative ions can escape the plasma at extremely high energy. For instance, having a cathode potential of 400 V, a negative oxygen ion can acquire a kinetic energy of 400 eV, which corresponds to a particle speed of ≈70 km s^{-1} in vacuum. Several issues can arise from negative-ion bombardment: etching of the substrate and implantation of ions in the subsurface of the deposited layer. The latter, because of the introduction of interstitial oxygen, has been presented as being one reason for the decrease in conductivity in n-type transparent conductive oxide.[17] To reduce negative-ion bombardment, a list of solutions has been proposed: the increase of the pressure, the reduction of the cathode potential, the increase of the distance between the target and the sample, or to adopt an off-axis deposition.[16]

Thus, the direct deposition of TMO on silicon by reactive sputtering might not be appropriate. It could produce a large number of defects, which can potentially pin the Fermi level and act as recombination center for electron/hole pairs, created in the silicon under illumination.[18,19]

In adition, to minimize the quantity of defect at the silicon/TMO interface, the insertion of a thin passivating silicon dioxide layer (2–3 nm[20]) might be beneficial to reduce the interface state density, particularly after hydrogen passivation.[20,21] Thus, charge-carrier lifetimes of 500 µs have been reported for bare

R. Poulain, Prof. A. Klein
Institute of Materials Science
Electronic Structure of Materials
Technische Universität Darmstadt
Otto-Berndt-Str. 3, 64287 Darmstadt, Germany
E-mail: aklein@esm.tu-darmstadt.de

R. Poulain, Prof. J. Proost
Materials and Process Engineering
Université Catholique de Louvain
Place du Levant 2, B-1348 Louvain-la-Neuve, Belgium

The ORCID identification number(s) for the author(s) of this article can be found under https://doi.org/10.1002/pssa.201900730.

DOI: 10.1002/pssa.201900730

Si/SiO_2 interfaces after hydrogen passivation.[22] In adition, the addition of alumina on top of the silicon dioxide layer could help to further improve the performance of the device.[23–25] We therefore studied TMO deposition on top of both hydrogen-passivated n-Si/SiO_2 and n-$Si/SiO_2/Al_2O_3$ substrates using X-ray photoelectron spectroscopy (XPS). XPS provides simultaneous information on the chemical nature of the surfaces and of the electronic structure.[26] It has the advantage that single interfaces can be studied, without the requirement of optimizing a device structure, in which many layers and patterns, e.g., for electrical characterization, are necessary.

Along with this article, we will see that during reactive sputtering of a TMO on silicon, the negatively charged oxygen ions deteriorate the interface. This is indicated by the formation of defect states in the SiO_2 layer, which induce a Fermi-level pinning and limit the band bending in the Si substrate. Defect formation and Fermi-level pinning can be avoided by growing the TMO sequentially using repeated sputtering and oxidation of a very thin metallic layer. We introduce this method as metal layer oxidation (MLO). We take as practical example, the deposition of p-type NiO on n-Si/SiO_2 and n-$Si/SiO_2/Al_2O_3$ substrates, as NiO could be implemented in numerous applications including silicon-based metal insulator semiconductor structure[3,4] and photoelectrochemical water-splitting devices.[1]

2. Results and Discussion

2.1. The Si 2p Spectra

The in situ XPS measurements of the Si 2p region display typically two emission structures, which can be associated to the silicon and the silicon dioxide layer, respectively. As seen in **Figure 1**, the elemental silicon peak is at lower binding energies. The peak is made of a double feature: a main peak Si_0 and a satellite peak, which are actually the photoemission of the spin-orbit split Si $2p_{3/2}$ and Si $2p_{1/2}$ components, respectively. At higher binding energies, the photoemission from the silicon in the SiO_2 layer is observed. This is labeled as Si^{IV} in Figure 1.

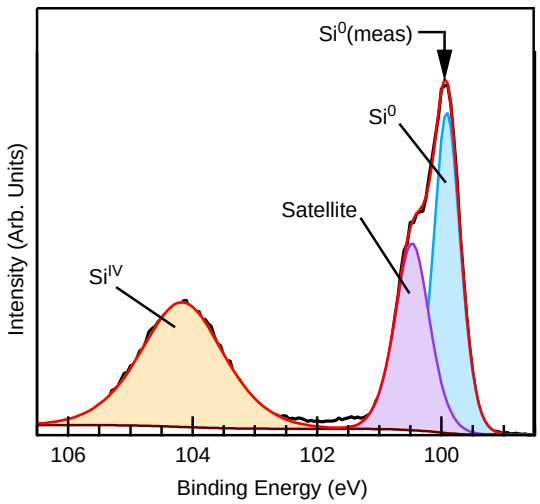

Figure 1. Typical XPS spectra of the Si 2p region. Two main features can be identified: the photoemission from the silicon dioxide layer on the surface (Si^{IV}) and the photoemission from the elemental silicon substrate. The elemental silicon is composed of a main peak Si^0 and a satellite peak, which are associated to the spin-orbit split Si $2p_{3/2}$ and Si $2p_{1/2}$ components, respectively. The Si^0(meas) arrow indicates the Si^0 peak position.

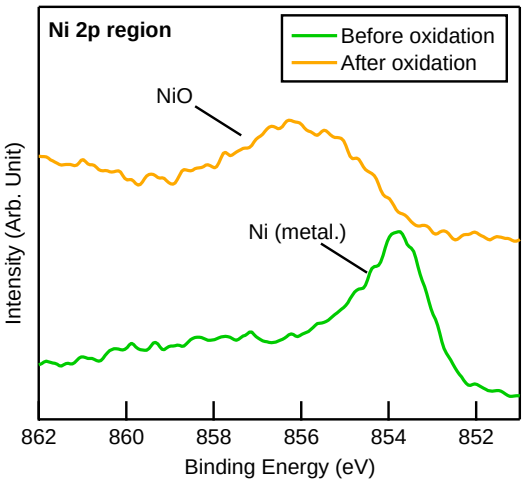

Figure 2. XP spectra of the Ni $2p_{3/2}$ region before and after exposition of a metallic nickel layer to an oxygen-rich atmosphere. The thickness of the final nickel oxide layer is about 0.3 Å.

2.2. Chemical Interface Properties

As observed in **Figure 2**, after the deposition by sputtering of nickel in oxygen-free atmosphere and before oxidation, the XPS spectra of the Ni 2p region displays a sharp peak which can be associated to elemental nickel Ni^0, and after exposition of the metallic layer in an oxygen-rich atmosphere, the peak is broadened and shifted to higher binding energy as a result of the oxidation of nickel into nickel oxide. No obvious trace of metallic nickel is visible. This result indicates that the metallic nickel layer is totally converted into nickel oxide after oxidation and so that the MLO method is able to produce a metal oxide layer.

The evolution of the Ni $2p_{3/2}$ emission in dependence on NiO film thickness is shown in **Figure 3**. The spectra are recorded during NiO growth using the MLO process. The spectra of the thickest layer shows the typical features of NiO with a main emission line near 854 eV and a characteristic satellite emission at 1.5–2 eV higher binding energies.[27,28] Identical spectra are obtained for magnetron-sputtered films. At lower film thickness, the spectra are broadened and have higher binding energies. Such a behavior is frequently observed in dependence on film thickness[28] and can be associated to the change in the local structure of the NiO layer.[29] The Si substrate intensity is attenuated exponentially in dependence on NiO film thickness, indicating a layer-by-layer growth and a conformal coverage of the NiO layer.

Photoelectron spectra recorded during stepwise growth of NiO onto Si/SiO_2 are shown in **Figure 4**. Three different experiments with NiO grown by metal-layer-oxidation, reactive direct current (DC), reactive sputtering, and radio frequencies (RF) sputtering are compared. The spectra are normalized to the Si^0 intensity for better comparison.

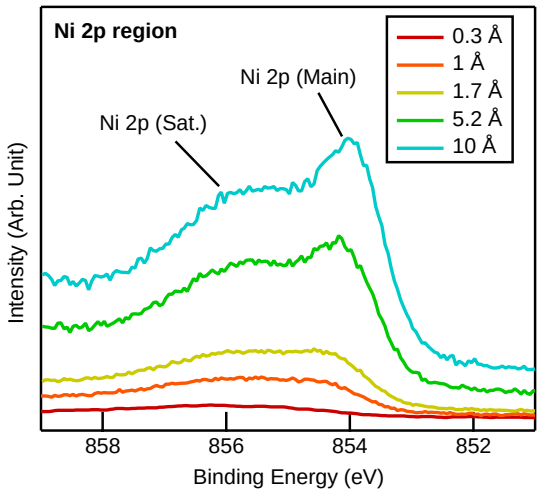

Figure 3. XP spectra of the Ni $2p_{3/2}$ region after exposure to oxygen of a thin metallic nickel layer deposited by sputtering in argon. The spectra are recorded for successive NiO layers.

The spectra in Figure 4 clearly show that a new emission arises between the Si^0 and the Si^{IV} peaks when NiO is deposited by reactive DC or RF magnetron sputtering. According to the literature, such intermediate emissions, which are labeled as Si^{def} in Figure 4, can be associated to the presence of noncompletely coordinated Si with intermediate oxidation states (Si^{I-III}).[30–33] Contrary to reactive sputtering, no Si^{def} emission is observed if the NiO is grown by the MLO method. The results indicate that Si^{def} only appears when oxygen is present during sputtering. This suggests that the Si^{def} emission is related to the bombardment of the substrate with negatively charged oxygen species formed in the plasma during deposition. For the reactively sputtering NiO films, the Si^{def} emissions increase with NiO film thickness, indicating that intensity is proportional to the exposure time of the surface to the plasma.

The maximum of the Si^{def} emission occurs at 58% of the distance between the Si^0 and the Si^{IV} peaks. Therefore, the Si^{def} state might correspond to the Si in the oxidation state +III state, which has been reported to occur at 62% of the distance between the Si^0 and the Si^{IV} peaks.[30]

The Si^{def} emissions may have a different origin: 1) they can result from an uncomplete reaction, after diffusion through the SiO_2 layer, of the incoming oxygen ions with the underneath silicon; 2) they could be related to surface etching of the silicon dioxide layer; or finally 3) they could be the fingerprint of the presence of interstitial oxygens in the the SiO_2 layer. The latter case (3) could eventually result in the formation of Si^{III} states under X-ray irradiation.[34]

Regarding case (1), it has to be mentioned that we also observed a comparable Si^{def} emission next to the Si^{IV} peak (Supporting Information, Figure 2) in the course of deposition of barium strontium titanate (BST: $(Ba,Sr)TiO_3$ on thick SiO_2 by RF sputtering in an $Ar:O_2$ (99:1) atmosphere. In this case, the oxygen source could be the target itself. This result suggests that Si^{def} state appears even when no metallic Si^0 is present in the substrate, indicating that the Si^{def} state is not related to the reaction of the elemental silicon Si^0 with the incoming oxygen ions. Therefore, case (1) is rather unlikely.

Cases (2) and (3) can be differentiated by comparing the intensity of the oxide emission in comparison with the intensity of the elemental silicon Si^0. For case 2) (etching of SiO_2), a reduction of the SiO_2 thickness has to be expected. Therefore, the intensity of the elemental silicon should increase in comparison with the Si^{IV} peak. On the contrary, at first sight, no substantial change of that intensity ratio is expected for case (3) (interstitial oxygen). To compare the relative area intensity, the ratio R_A between the area of the oxide (A_{oxide}), which includes the Si^{IV} and the Si^{def} states, and the elemental silicon ($A_{silicon}$) is introduced

$$R_A = \frac{A_{oxide}}{A_{silicon}} \quad (1)$$

The evolution of the ratio R_A with NiO thickness is displayed for the different deposition methods in **Figure 5**. The result

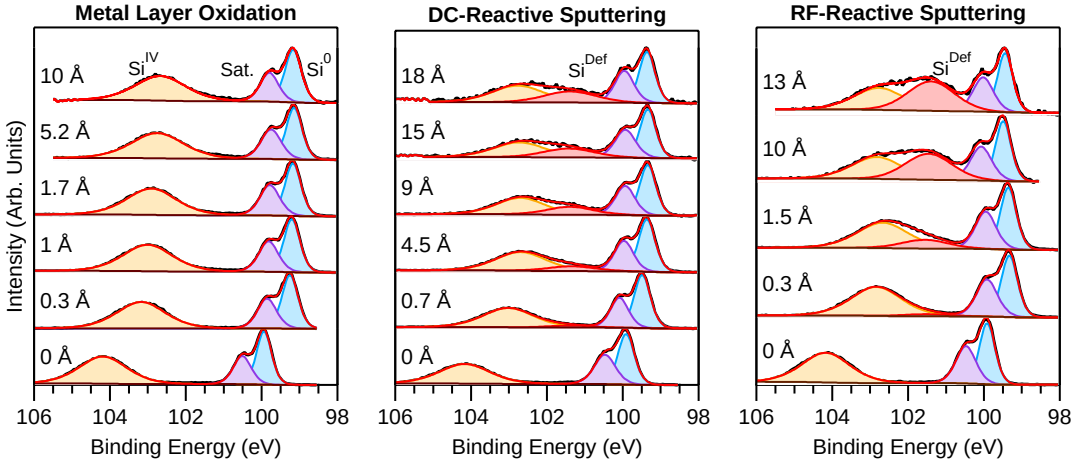

Figure 4. Si 2p spectra measured by XPS during the interface experiments with NiO on Si/SiO_2 substrates. Three deposition method have been evaluated: MLO, DC reactive sputtering, and RF reactive sputtering. The spectra are normalized to the Si^0 intensity for better comparison of the evolution of the peak shapes.

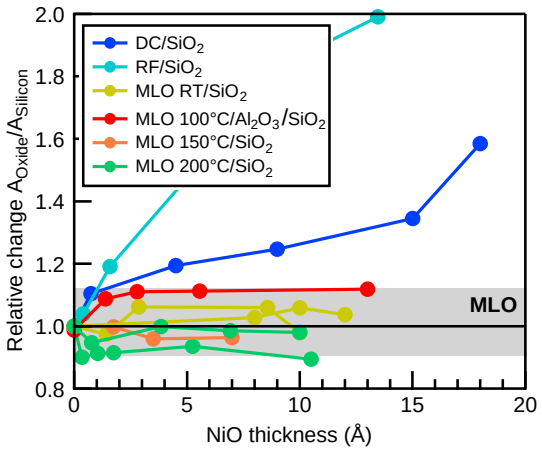

Figure 5. Evolution of the ratio of the oxide area (Si^{IV} and Si^{def}) over the elemental silicon area Si^0 for the different NiO deposition methods. Values are normalized against the value obtained before NiO deposition.

clearly indicates that the ratio R_A increases with NiO thickness for both reactive sputtering methods. This trend discards etching of SiO_2 as origin of the Si^{def} states. This is consistent with the relatively high pressure used for the DC and RF sputtering, which favors thin-film deposition in the Keller–Simmon regime, where no etching of the surface is expected.[16]

The data in Figure 5 also show that the ratio R_A does not significantly change when NiO is prepared by the MLO method, contrary to what can be obtained with reactive sputtering. This indicates that the MLO method preserves the Si/SiO_2 interface integrity relatively well.

Although a more complicated situation might also account for the Si^{def} states, our analysis suggests that these states are related to the presence of oxygen interstitial in the silicon dioxide layer (case 3). This proposition is supported by the work of Chen et al.,[34] who showed using density functional theory calculations that oxygen interstitials in SiO_2 are the origin of numerous defective structures, which can be stabilized along the oxygen bridging bonded (OBB) structure

$$\equiv Si - \overset{\overset{Oi}{|}}{O} - Si \equiv \quad (2)$$

The OBB structure might convert into a peroxy radical (POR) structure where the bond between the silicon and the oxygen (Si—O) is broken when exposed to irradiation (e.g., X-rays).[34] In the POR structure, the silicon atom would be bonded by three covalent pairs only to the silicon dioxide structure. Therefore, the Si^{def} state observed in this work may be associated to a POR structure, which should exhibit a binding energy corresponding to Si^{III} in XPS.

2.3. Electronic Interface Properties

Interface experiments such as those shown in Figure 4 aim at determining the built-in voltage (V_{bi}) in the silicon substrate of the Si/SiO_2/NiO interface. However, the observed binding-energy shifts of the Si 2p emission do not necessarily correspond to the built-in voltage. The observed shift can be smaller, as a photovoltage U_{ph} can be induced by the electron–hole pairs generated by the X-ray irradiation.[35] The binding energy of the elemental Si relative to the calculated flat-band position ($\Delta E_b(Si^0)$) then corresponds to

$$\Delta E_b(Si^0) = E_{fb}(Si^0) - E_b(Si^0) = q(V_{bi} - U_{ph}) \quad (3)$$

where q is the charge of the electron. Following the calculations described by Schafranek et al.,[36] which describe measurements in the same setup, the photovoltage in silicon can be estimated for a built-in voltage V_{bi} varying from 0 to 0.9 V. In **Figure 6**, the relationship between the measured peak deviation $\Delta E_b(Si^0)$ in dependence on built-in voltage is shown. It shows two different regimes: a linear dependence of $\Delta E_b(Si^0)$ on V_{bi} for $V_{bi}<0.6$ V and a saturation regime where $\Delta E_b(Si^0) \approx 0.62$ eV for $V_{bi}>0.6$ V. The development of the photovoltage causes a saturation of the observable binding-energy shifts. Consequently, $\Delta E_b(Si^0)$ measured by XPS is only directly correlated to the built-in voltage if the value is smaller than ≈0.6 V. Larger built-in voltages can not be identified any more. Therefore, if the observed binding energy of the Si^0 emission is 0.6 eV higher than that of the flat-band position, it can only be said that the built-in voltage is 0.6 V or higher.

The binding energies of the Si^0 emission of hydrogen-passivated Si/SiO_2 substrates are shown in dependence on NiO film thickness in **Figure 7**. After hydrogen passivation, the binding energy of the Si peak $E_b(Si^0)$ is close to 99.6–99.7 eV (Figure 7). The flat-band position ($E_{fb}(Si^0)$), where no charge accumulation (negative or positive) occurs at the silicon surface, is calculated to be 99.57 ± 0.05 eV when the bulk Fermi level and the binding energy of the Si^0 emission with respect to the valence-band maximum are taken as 0.83 eV (see Section 2) and 98.74 eV,[37] respectively. Therefore, the measurements suggest that passivated Si/SiO_2 samples are slightly accumulating negative charges at the silicon surface (Figure 7). This would imply that not all trapped charges are suppressed after hydrogen passivation. However, the hydrogen passivation step was found to remove contaminants and to reduce substantially the accumulation of charges at the Si/SiO_2 interface (see Supporting

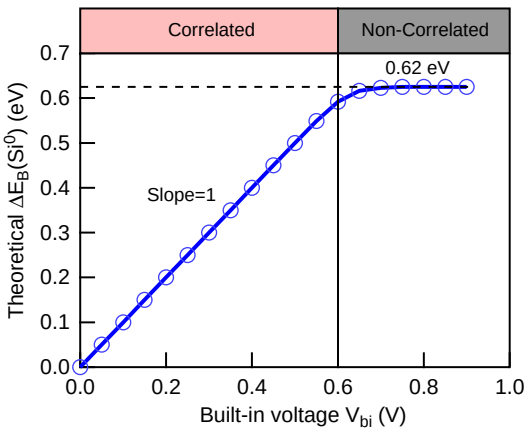

Figure 6. Calculated the peak deviation $\Delta E_b(Si^0)$ (Equation (3)). For built-in voltages $V_{bi}>0.6$ eV, the peak deviation saturates due to the development of a photovoltage induced by the X-ray source.

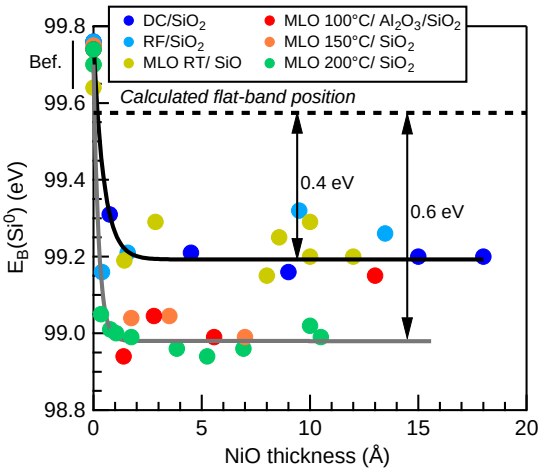

Figure 7. Binding energy of Si^0 peak during interface formation of n-Si/SiO_2 substrates with differently deposited NiO in dependence on NiO film thickness. The Si^0 binding energies of the uncovered, hydrogen passivated samples are slightly above the calculated flat-band position. It suggests that negative charges accumulate at the interface. The label Bef. stands for Before and aim at emphasizing the position of the Si^0 before the deposition of NiO.

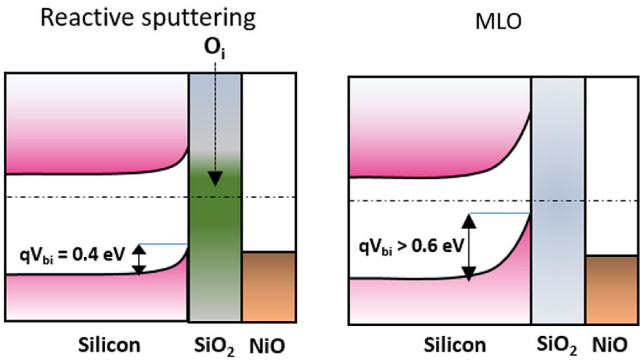

Figure 8. Band-diagram representing the $Si/SiO_2/NiO$ junction when NiO is deposited by reactive sputtering (left) or by metal-layer-oxidation (right). The silicon band-bending is pinned at 0.4 eV for reactively sputtered NiO due to the presence of oxygen interstitial (O_i), while it might exceed 0.6 eV if NiO is prepared by the MLO method.

Information, Figure 1). The accumulation of negative charge after the hydrogen passivation step can arise because of the presence of positive trapped charges at the Si/SiO_2 interface [38–40] or in the SiO_2 layer.[34,41,42]

Figure 7 shows that the position of the Si^0 peak shifts to lower binding energy for any deposition method, indicating that the deposition of NiO leads to the formation of a depletion layer in the silicon with a built-in voltage $V_{bi}>0$. The binding energies at the interfaces with RF and DC sputtered NiO saturate at ≈99.2 eV, corresponding to a built-in potential of 0.4 V. This value is in line with what has been reported in the literature.[1] In contrast, the binding energies obtained when NiO is deposited by MLO at $T > 100$ °C saturate at ≈99.0 eV, which is 0.6 eV lower than the expected value for the flat-band condition. As discussed earlier (see Figure 6), it can then only be said that the built-in voltage V_{bi} in the silicon is at least 0.6 eV.

The interface experiments highlight that larger Si^0 peak deviation is attained with the MLO method if sufficient temperature is brought to the substrate during the oxidation step (Figure 7). A lower peak deviation, comparable with that for reactively sputtered NiO, is observed when NiO is deposited by MLO with the oxidation step being carried out at room temperature. This lower V_{bi} could be due to an incomplete surface reaction of the metallic nickel with oxygen during the oxidation step or due the formation of a nonhomogeneous material. It is mentioned that $\Delta E_b(Si^0)$ is also ≈0.6 eV, when a thin ALD Al_2O_3 layer is inserted between the silicon dioxide and the nickel oxide layer. This can be particularly interesting as it has been reported that tunneling SiO_2/Al_2O_3 structures on top of silicon might provide better device performance.[23–25] In addition, it could be assumed that the alumina layer may be used as a diffusion-blocking layer to avoid degradation over time, by the reaction of hydrogen from the hydrogen-passivated SiO_2 layer and the reduction of the NiO layer.

Finally, as depicted in **Figure 8**, the limited Si^0 deviation when NiO is deposited by reactive sputtering could be associated to the presence of oxygen interstitials in the silicon dioxide layer, resulting from the intense bombardment of the surface by energetic ionized oxygen particles during deposition. In comparison with the results obtained by MLO, the defects produced during NiO deposition by reactive sputtering would pin the Fermi energy in a nondesired position. Therefore, to produce a high-quality interface of a TMO by sputtering on Si/SiO_2 substrates, the results presented in this article would suggest that it is preferable to start from a metallic target, to sputter, without oxygen, a thin metallic layer (<1 nm), and to oxidize by exposing the metallic layer to oxygen without the plasma. For practical use, this method can be referred as MLO.

3. Conclusion

Along with this article, an alternative to reactive sputtering has been presented to interface thin TMO layers (<5 nm) with Si/SiO_2. The deposition consisted of the growth of thin metallic (nickel) layers (<1 nm) in oxygen-free atmosphere followed by a subsequent oxidization step in oxygen without plasma, where the addition of thermal energy during the oxidation process might increase the TMO layer quality. Named MLO, the method has the advantage to avoid direct surface exposition to negative oxygen ion bombardment as for DC and RF reactive sputtering.

Thus, the band deviation in silicon has been estimated to be at least 0.6 eV when passivated Si/SiO_2 substrate is interfaced with nickel oxide by the MLO method. On the contrary, DC and RF reactive sputtering processes provide a more limited band-bending (≈0.4 eV). The results suggest that reactive sputtering pins the bands in an undesired position as a consequence of the intense bombardment by negative oxygen ions of the Si/SiO_2 interface which might implant oxygen interstitial in the SiO_2 layer.

4. Experimental Section

Base Substrate: Experiments were realized with n-type float-zone silicon single crystal (100) wafers with sheet resistivity 10.1 Ω cm determined by

the van der Pauw method. The doping concentration was estimated to be 4.4×10^{14} cm^{-3}, corresponding to bulk Fermi-level position of 0.834 eV above the valence-band maximum.

Cleaning: To ensure a clean surface free of any carbon or oxygen species, the samples were processed in a piranha (H_2O_2:H_2SO_4 5:2) bath followed by a fluoridic acid (HF 2%) treatment. The samples were extensively rinsed with DI water between each bath and at the end. After the chemical bath, a hydrophobic silicon surface was obtained, which was a clue of an H-terminated oxide-free silicon surface.

Silicon Dioxide Growth: Immediately after the cleaning step, an ≈2.3–2.5 nm amorphous silicon dioxide layer, compatible with electrical tunneling,[20,43] was thermally grown in a Koyo VP1000 furnace. After purging the chamber with nitrogen, the furnace temperature was cycled from 700 to 1000 °C in dry nitrogen atmosphere (99.99995% purity). It was believed that oxygen participating in the SiO_2 growth process originated from oxygen desorption from the furnace wall during the thermal cycling.

Hydrogen Cleaning and Surface Passivation: A hydrogen plasma source (Tectra Gen2 Hybrid Atom/Ion Source) was used for both surface cleaning and passivation of the Si/SiO_2 samples. Atomic hydrogen was obtained by cracking dihydrogen molecules in a plasma chamber set on atomic mode, for which the current was set to 30 mA and the gas pressure was set to 0.2 mbar. The hydrogen cleaning step was performed at ≈250 °C substrate temperature for 10 min. It allowed to remove efficiently the surface contaminants (hydrocarbons, water, etc.) originating from sample exposure to air during the transfer from the furnace to the vacuum system. Following reports in the literature,[30,44] an additional 45 min hydrogen plasma exposure was carried out at higher temperature (350 °C) for the hydrogen passivation step. To avoid possible hydrogen desorption from the sample, the plasma is maintained until the sample holder temperature reaches 150 °C.

Alumina Deposition: ALD-alumina was deposited by the alternative deposition and oxidation by water of TMA at 50 °C.[45] Low-temperature deposition was selected to avoid any SiO_2 depassivation reaction. TMA and water pulses lasted for 80 and 150 ms, respectively, and were separated by an evacuation period of 5 min. The first pulse started with TMA. Overall, ten TMA pulses were realized. After the ALD deposition, another hydrogen cleaning and hydrogen passivation step were processed as previously described.

Deposition of NiO: The deposition of nickel oxide on the Si/SiO_2 substrates had been realized by DC and RF reactive sputtering in 5% O_2 and target-to-substrate distance of 13 cm. The pressure was set to 6 and 1 Pa for DC and RF sputtering, respectively. The MLO process had been realized in similar conditions except that a metallic nickel layer was DC sputtered in oxygen-free atmosphere, which was then followed by an in situ post oxidation step without plasma exposure. The oxidation of the metallic nickel in the growth chamber works relatively well for the thickness of less than 1 nm. The oxidation process was tested for gas pressures between 1 and 6 Pa using processing gases with 10% and 100% oxygen content and various temperatures from RT to 200 °C. All conditions provided a fully oxidized NiO layer as confirmed by XPS.

In situ Analysis: Interface analysis using XPS was realized in the DAISY-MAT (Darmstadt Integrated System for Materials Research) system in which the electron spectrometer (Physical Electronics PHI 5700) was connected to various vacuum chambers hosting the remote plasma source, the ALD system, and the sputter deposition.[26] Samples can be transferred to the different places without breaking the vacuum, which eliminates any surface contamination during the experiments.

XPS Measurements: All XPS measurements were realized with a 1486.6 eV Al Kα monochromatic X-ray and 45° take-off angle to the sample. Binding energies were referenced to the Fermi level, which was calibrated beforehand against a clean silver surface.

Supporting Information

Supporting Information is available from the Wiley Online Library or from the author.

Acknowledgements

This work was funded by the European Union's Horizon 2020 research and innovation programme under the Marie Sklodowska-Curie grant agreement No. 641640 (EJD-ITN project FunMAT). The authors also cordially thank the technical team of the Wallonia Infrastructure for Nano FABrication (Winfab) platform.

Conflict of Interest

The authors declare no conflict of interest.

Keywords

Fermi-level pinning, interface passivation, NiO, photoemission, Si

Received: August 31, 2019
Revised: October 3, 2019
Published online: November 8, 2019

[1] S. Tengeler, M. Fingerle, W. Calvet, C. Steinert, B. Kaiser, T. Mayer, W. Jaegermann, *J. Electrochem. Soc.* **2018**, *165*, H3122.
[2] L. G. Gerling, S. Mahato, A. Morales-Vilches, G. Masmitja, P. Ortega, C. Voz, R. Alcubilla, J. Puigdollers, *Sol. Energy Mater. Solar Cells* **2016**, *145*, 109.
[3] R. Islam, P. Ramesh, N. J. Hyung, K. C. Saraswat, in *Proceedings of the 2015 IEEE 42nd Photovoltaic Specialist Conference*. IEEE, New Orleans, LA, USA, **2015**, pp. 1–4.
[4] R. Islam, G. Shine, K. C. Saraswat, *Appl. Phys. Lett.* **2014**, *105*, 182103.
[5] X. Yang, Q. Bi, H. Ali, K. Davis, W. V. Schoenfeld, K. Weber, *Adv. Mater.* **2016**, *28*, 5891.
[6] R. Pietruszka, B. S. Witkowski, S. Gieraltowska, P. Caban, L. Wachnicki, E. Zielony, K. Gwozdz, P. Bieganski, E. Placzek-Popko, M. Godlewski, *Sol. Energy Mater. Solar Cells* **2015**, *143*, 99.
[7] C. Battaglia, S. M. de Nicolas, S. De Wolf, X. T. Yin, M. Zheng, C. Ballif, A. Javey, *Appl. Phys. Lett.* **2014**, *104*, 5.
[8] M. Bivour, C. Messmer, L. Neusel, F. Zähringer, J. Schön, S. W. Glunz, M. Hermle, in *33rd European PV Solar Energy Conference and Exhibition*, Amsterdam **2017**, pp. 348–352.
[9] W. Lin, W. Wu, Q. Xie, Z. Liu, K. Qiu, L. Cai, Z. Yao, L. Meng, B. Ai, Z. Liang, H. Shen, *ACS Appl. Mater. Interfaces* **2018**, *10*, 43699.
[10] L. D'Amario, G. Boschloo, A. Hagfeldt, L. Hammarstrom, *J. Phys. Chem. C* **2014**, *118*, 19556.
[11] K. X. Steirer, J. P. Chesin, N. E. Widjonarko, J. J. Berry, A. Miedaner, D. S. Ginley, D. C. Olson, *Org. Electron.* **2010**, *11*, 1414.
[12] M. D. Irwin, J. D. Servaites, D. B. Buchholz, B. J. Leever, J. Liu, J. D. Emery, M. Zhang, J. H. Song, M. F. Durstock, A. J. Freeman, M. J. Bedzyk, M. C. Hersam, R. P. H. Chang, M. A. Ratner, T. J. Marks, *Chem. Mater.* **2011**, *23*, 2218.
[13] S. Y. Liu, R. Liu, Y. Chen, S. H. Ho, J. H. Kim, F. So, *Chem. Mater.* **2014**, *26*, 4528.
[14] H. Sarı, H. Sakakura, D. Kawade, M. Itagaki, M. Sugiyama, *Thin Solid Films* **2015**, *592*, 150.
[15] H. Kanda, A. Uzum, A. K. Baranwal, T. A. N. Peiris, T. Umeyama, H. Imahori, H. Segawa, T. Miyasaka, S. Ito, *J. Phys. Chem. C* **2016**, *120*, 28441.
[16] K. Ellmer, T. Welzel, *J. Mater. Res.* **2012**, *27*, 765.
[17] D. Mergel, W. Stass, G. Ehl, D. Barthel, *J. Appl. Phys.* **2000**, *88*, 2437.
[18] M. Hermle, in *Photovoltaic Solar Energy: From Fundamentals to Applications*, Wiley, Chichester **2016**, pp. 125–135.

[19] Y. C. Yeo, P. Ranade, T. J. King, C. M. Hu, *IEEE Electron Dev. Lett.* **2002**, *23*, 342.
[20] J. Robertson, *Eur. Phys. J. Appl. Phys.* **2004**, *28*, 265.
[21] A. G. Aberle, *Prog. Photovolt.* **2000**, *8*, 473.
[22] G. Bourret-Sicotte, P. Hamer, R. S. Bonilla, K. Collett, P. R. Wilshaw, *Energy Procedia* **2017**, *124*, 267.
[23] R. Kotipalli, R. Delamare, O. Poncelet, X. Tang, L. A. Francis, D. Flandre, *EPJ Photovolt.* **2013**, *4*, 45107.
[24] I. A. Digdaya, G. W. P. Adhyaksa, B. J. Trzesniewski, E. C. Garnett, W. A. Smith, *Nat. Commun.* **2017**, *8*, 15968.
[25] G. Dingemans, F. Einsele, W. Beyer, M. C. M. van de Sanden, W. M. M. Kessels, *J. Appl. Phys.* **2012**, *111*, 093713.
[26] A. Klein, *J. Am. Ceram. Soc.* **2016**, *99*, 369.
[27] J. Y. Zhang, W. W. Li, R. L. Z. Hoye, J. L. MacManus-Driscoll, M. Budde, O. Bierwagen, L. Wang, Y. Du, M. J. Wahila, L. F. J. Piper, T. L. Lee, H. J. Edwards, V. R. Dhanak, K. H. L. Zhang, *J. Mater. Chem. C* **2018**, *6*, 2275.
[28] D. M. Long, A. Klein, E. C. Dickey, *Appl. Surf. Sci.* **2019**, *466*, 472.
[29] D. Alders, F. C. Voogt, T. Hibma, G. A. Sawatzky, *Phys. Rev. B* **1996**, *54*, 7716.
[30] B. Stegemann, A. Schoepke, D. Sixtensson, B. Gorka, T. Lussky, M. Schmidt, *Physica E* **2009**, *41*, 1019.
[31] F. Rochet, C. Poncey, G. Dufour, H. Roulet, C. Guillot, F. Sirotti, *J. Non Crystal Solids* **1997**, *216*, 148.
[32] P. J. Grunthaner, M. H. Hecht, F. J. Grunthaner, N. M. Johnson, *J. Appl. Phys.* **1987**, *61*, 629.
[33] F. J. Grunthaner, P. J. Grunthaner, R. P. Vasquez, B. F. Lewis, J. Maserjian, A. Madhukar, *J. Vac. Sci. Technol.* **1979**, *16*, 1443.
[34] Z. H. Chen, J. W. Wang, Y. Song, X. Zuo, *AIP Adv.* **2017**, *7*, 105118.
[35] M. Alonso, R. Cimino, K. Horn, *Phys. Rev. Lett.* **1990**, *64*, 1947.
[36] R. Schafranek, S. Payan, M. Maglione, A. Klein, *Phys. Rev. B* **2008**, *77*, 195310.
[37] R. Fritsche, E. Wisotzki, A. B. M. O. Islam, A. Thissen, A. Klein, W. Jaegermann, R. Rudolph, D. Tonti, C. Pettenkofer, *Appl. Phys. Lett.* **2002**, *80*, 1388.
[38] S. H. Lee, M. F. Bhopal, D. W. Lee, S. H. Lee, *Mater. Sci. Semicond. Process.* **2018**, *79*, 66.
[39] C. Herring, N. M. Johnson, C. G. Van de Walle, *Phys. Rev. B* **2001**, *64*, 125209.
[40] D. J. Chadi, *Phys. Rev. B* **2001**, *64*, 195403.
[41] C. J. Nicklaw, Z. Y. Lu, D. M. Fleetwood, R. D. Schrimpf, S. T. Pantelides, *IEEE Trans. Nuclear Sci.* **2002**, *49*, 2667.
[42] K. Kajihara, L. Skuja, H. Hosono, *J. Phys. Chem. C* **2014**, *118*, 4282.
[43] J. Bullock, D. Yan, A. Cuevas, B. Demaurex, A. Hessler-Wyser, S. De Wolf, in Proceedings of the 2014 IEEE 40th Photovoltaic Specialist Conference, IEEE, Denver, CO, USA **2014**, pp. 3442–3447.
[44] H. Angermann, O. Gref, B. Stegemann, *Central Eur. J. Phys.* **2011**, *9*, 1472.
[45] T. J. M. Bayer, A. Wachau, A. Fuchs, J. Deuermeier, A. Klein, *Chem. Mater.* **2012**, *24*, 4503.